BEILSTEIN JOURNAL OF NANOTECHNOLOGY

Supporting Information

for

Hierarchical Bi_2WO_6/TiO_2-nanotube composites derived from natural cellulose for visible-light photocatalytic treatment of pollutants

Zehao Lin, Zhan Yang and Jianguo Huang

Beilstein J. Nanotechnol. **2022,** *13,* 745–762. doi:10.3762/bjnano.13.66

Additional figures

Table S1: The dosages of $Bi(NO_3)_3 \cdot 5H_2O$ and $Na_2WO_4 \cdot 2H_2O$ reagents in the preparation processes of the hierarchical Bi_2WO_6/TiO_2-NT nanocomposites.

Nanocomposites	$Bi(NO_3)_3 \cdot 5H_2O$/mg	$Na_2WO_4 \cdot 2H_2O$/mg
30%−Bi_2WO_6/TiO_2-NT	23.8	8.1
50%−Bi_2WO_6/TiO_2-NT	55.6	18.9
70%−Bi_2WO_6/TiO_2-NT	129.7	44.1
90%−Bi_2WO_6/TiO_2-NT	500.3	170.2

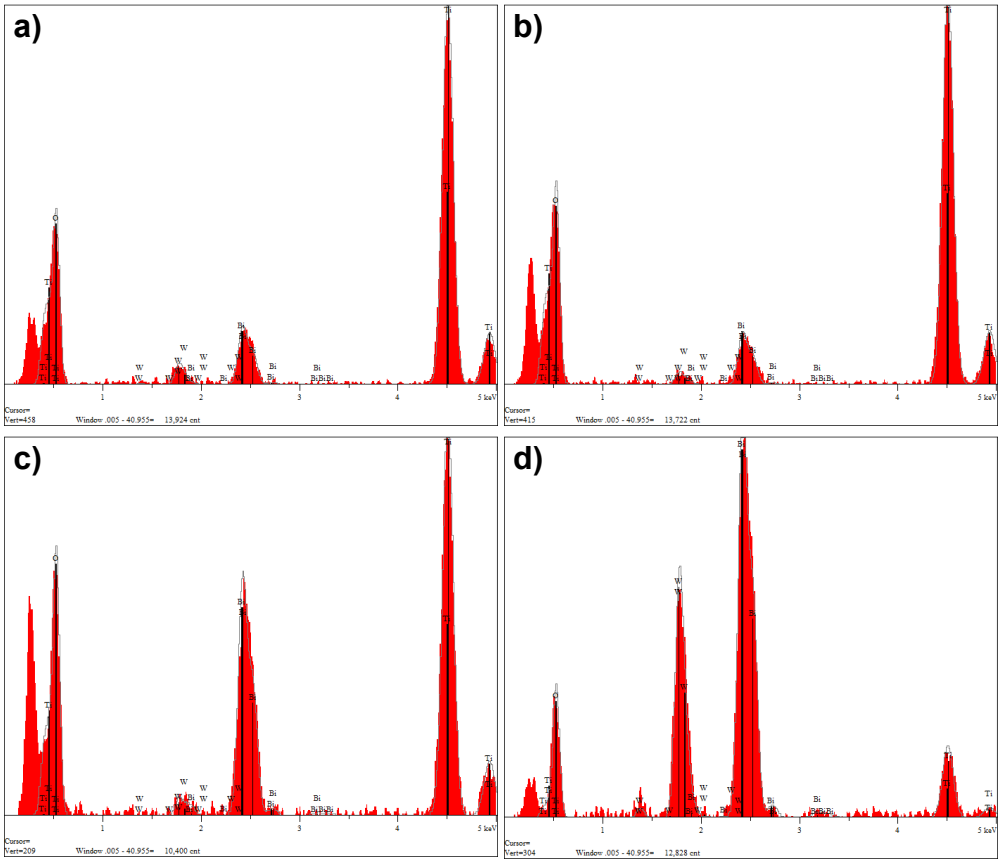

Figure S1: EDX spectra of the hierarchical (a) 30%−Bi_2WO_6/TiO_2-NT, (b) 50%−Bi_2WO_6/TiO_2-NT, (c) 70%−Bi_2WO_6/TiO_2-NT, and (d) 90%−Bi_2WO_6/TiO_2-NT nanocomposites.

Table S2: Practical mass contents of Ti and Bi elements, as well as the Bi_2WO_6 component in the hierarchical Bi_2WO_6/TiO_2-NT nanocomposites.

Nanocomposites	Practical mass content of Ti/wt %	Practical mass content of Bi/wt %	Practical mass content of Bi_2WO_6/wt %
30%−Bi_2WO_6/TiO_2-NT	47.04	29.26	38.4
50%−Bi_2WO_6/TiO_2-NT	37.56	44.52	54.3
70%−Bi_2WO_6/TiO_2-NT	22.40	60.29	72.9
90%−Bi_2WO_6/TiO_2-NT	3.79	74.50	95.2

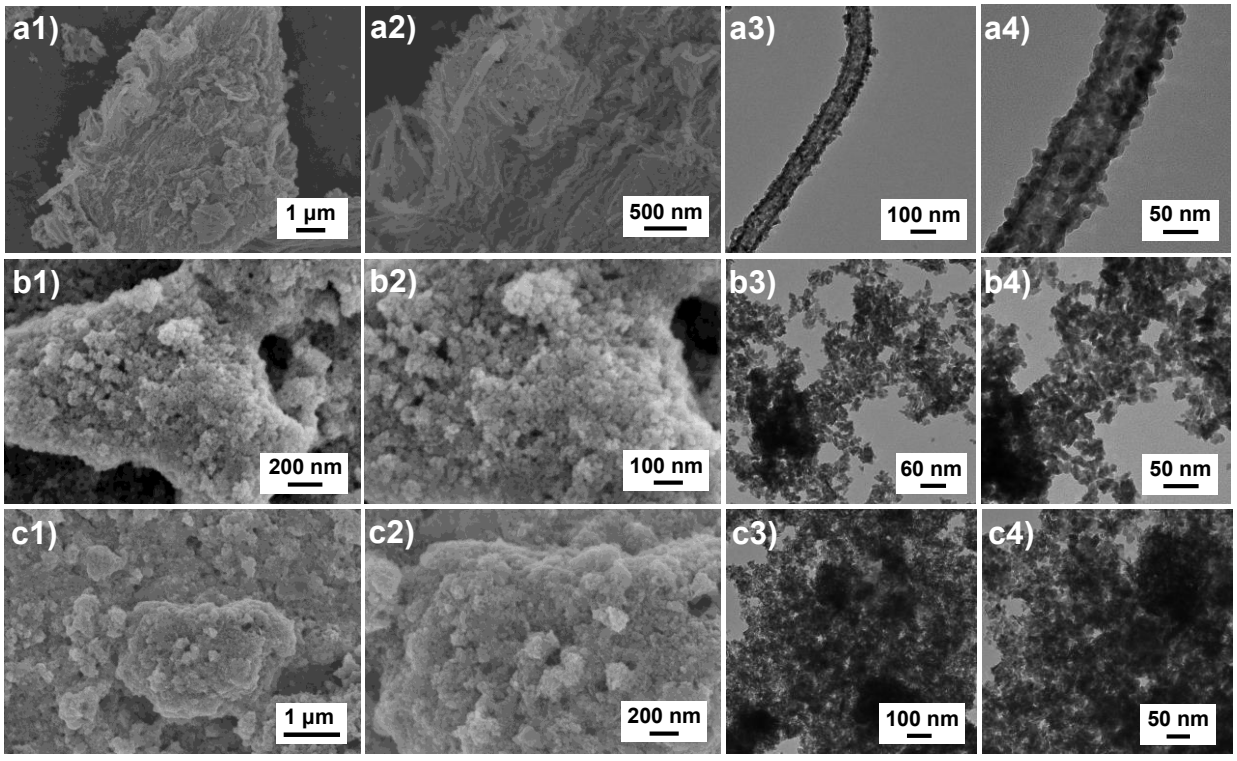

Figure S2: Electron micrographs of the (a1−a4) pure TiO_2-NT sample, (b1−b4) pure Bi_2WO_6 powder sample, and (c1−c4) the Bi_2WO_6/TiO_2 sample prepared without the cellulose template. The first two columns represent the FE-SEM images, and the last two columns exhibit the TEM images of the corresponding samples.

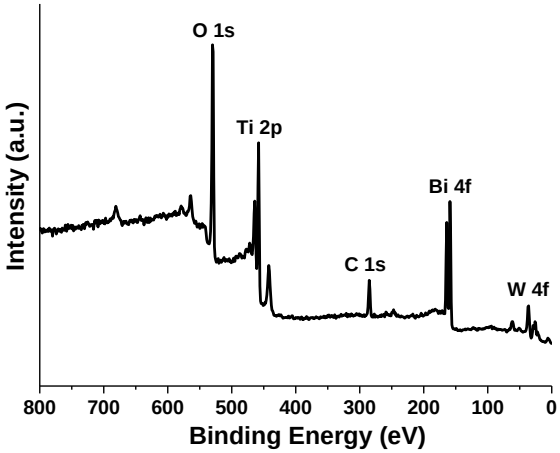

Figure S3: XPS survey spectrum of the hierarchical 70%−Bi_2WO_6/TiO_2-NT nanocomposite.

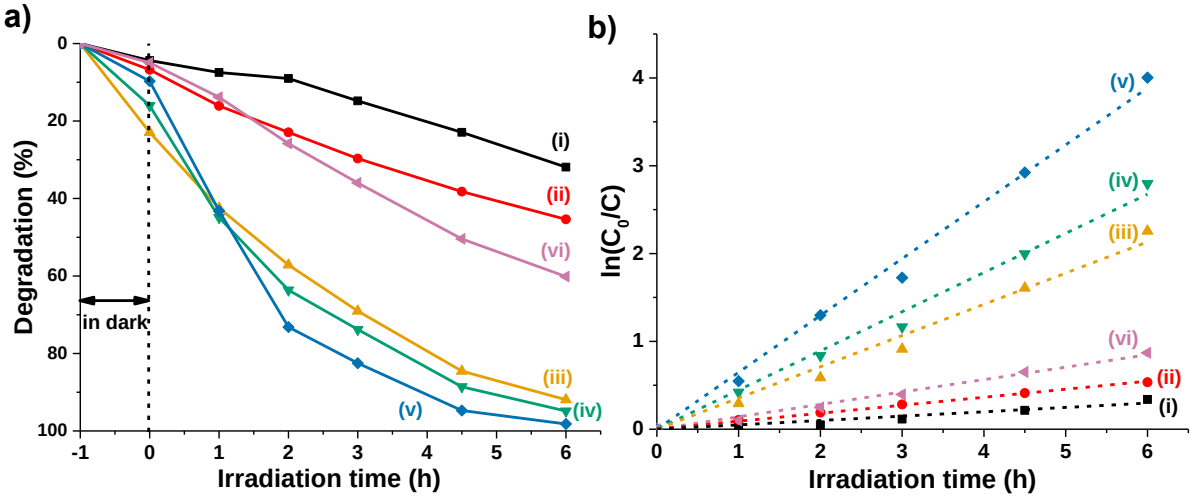

Figure S4: (a) The visible-light (λ > 420 nm) induced photocatalytic degradation profiles and (b) the corresponding linear fitting curves based on the pseudo-first-order kinetic model towards the photodegradation of RhB pollutant solution (10 $mg \cdot L^{-1}$) by the (i) pure TiO_2-NT,

(ii) pure Bi_2WO_6 powder, as well as the hierarchical (iii) 30%−Bi_2WO_6/TiO_2-NT, (iv) 50%−Bi_2WO_6/TiO_2-NT, (v) 70%−Bi_2WO_6/TiO_2-NT, and (vi) 90%−Bi_2WO_6/TiO_2-NT nanocomposites.

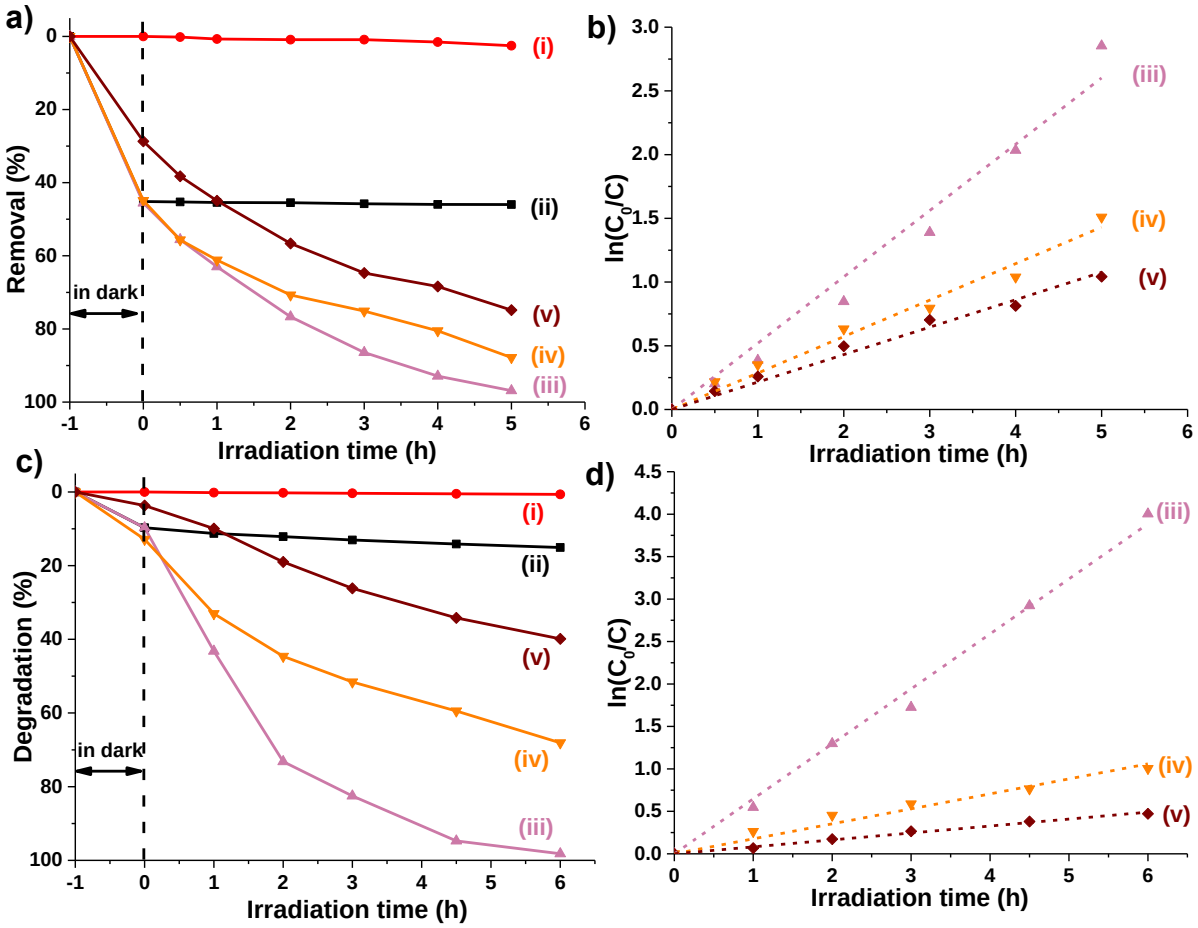

Figure S5: (a) The reduction profiles towards Cr(VI) pollutant solution (10 mg·L^{-1}, pH 4) and (c) the degradation profiles towards RhB pollutant solution (10 mg·L^{-1}) as well as (b,d) the corresponding linear fitting curves based on the pseudo-first-order kinetic model under different conditions. (i) The self-reduction reaction of Cr(VI) or self-degradation reaction of RhB without photocatalysts under visible-light (λ > 420 nm) irradiation. (ii) The self-adsorption by the hierarchical 70%−Bi_2WO_6/TiO_2-NT nanocomposite towards Cr(VI) or RhB pollutant solution. And the visible-light (λ > 420 nm) induced photocatalytic reactions towards Cr(VI) or RhB pollutant solution by employing (iii) the hierarchical 70%−Bi_2WO_6/TiO_2-NT

nanocomposite, (iv) the Bi_2WO_6/TiO_2 sample prepared without the cellulose template, and (v) the Bi_2WO_6-TiO_2 sample prepared by physical blend as the photocatalysts.

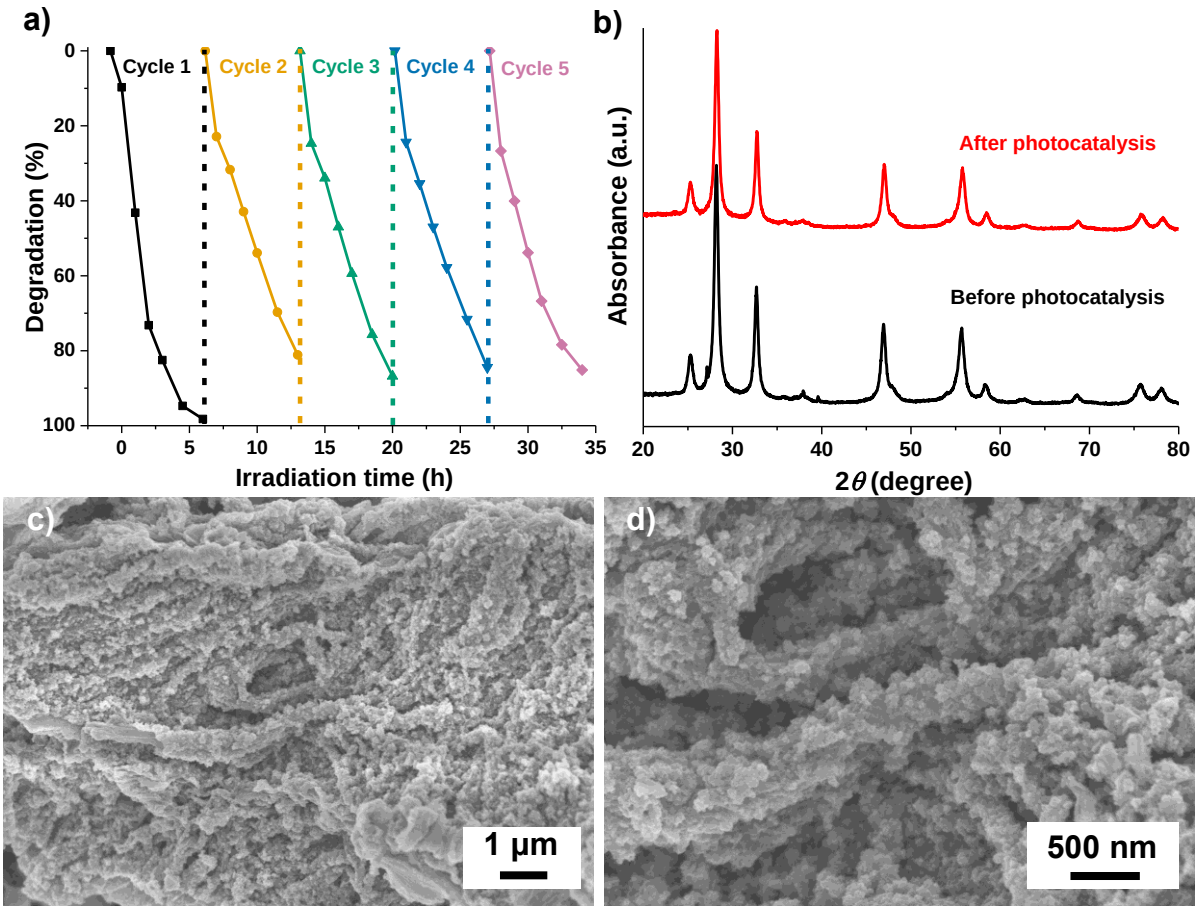

Figure S6: (a) The visible-light (λ > 420 nm) induced photocatalytic degradation profiles towards the photodegradation of RhB pollutant solution (10 $mg \cdot L^{-1}$) for five cycles by the hierarchical 70%−Bi_2WO_6/TiO_2-NT nanocomposite. (b) The XRD patterns of the 70%−Bi_2WO_6/TiO_2-NT nanocomposites before and after 5-cycle photocatalysis. (c,d) The FE-SEM images of the 70%−Bi_2WO_6/TiO_2-NT nanocomposite after 5-cycle photocatalysis.

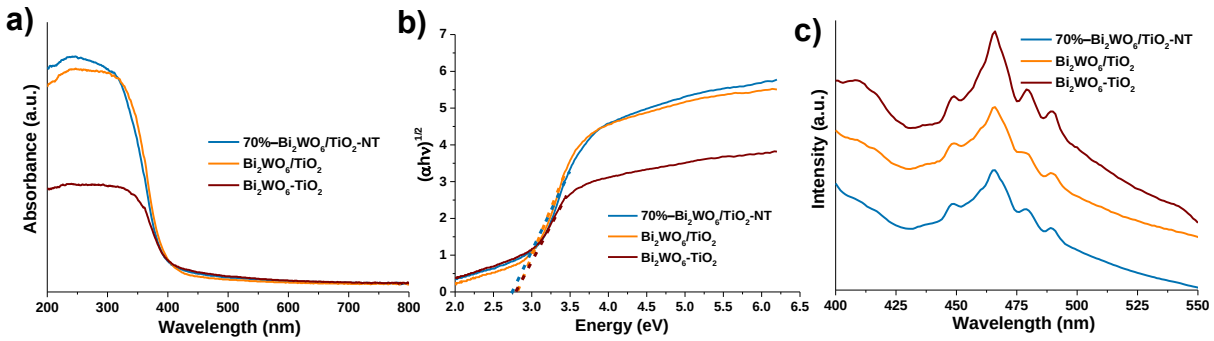

Figure S7: (a) The UV–vis DRS, (b) the band gaps determined by the intercept on the *x*-axis of the respective Tauc plots, and the PL emission spectra under the excitation of 360 nm of the hierarchical 70%−Bi_2WO_6/TiO_2-NT nanocomposite, the Bi_2WO_6/TiO_2 sample prepared without the cellulose template, and the Bi_2WO_6-TiO_2 sample prepared by physical blend.

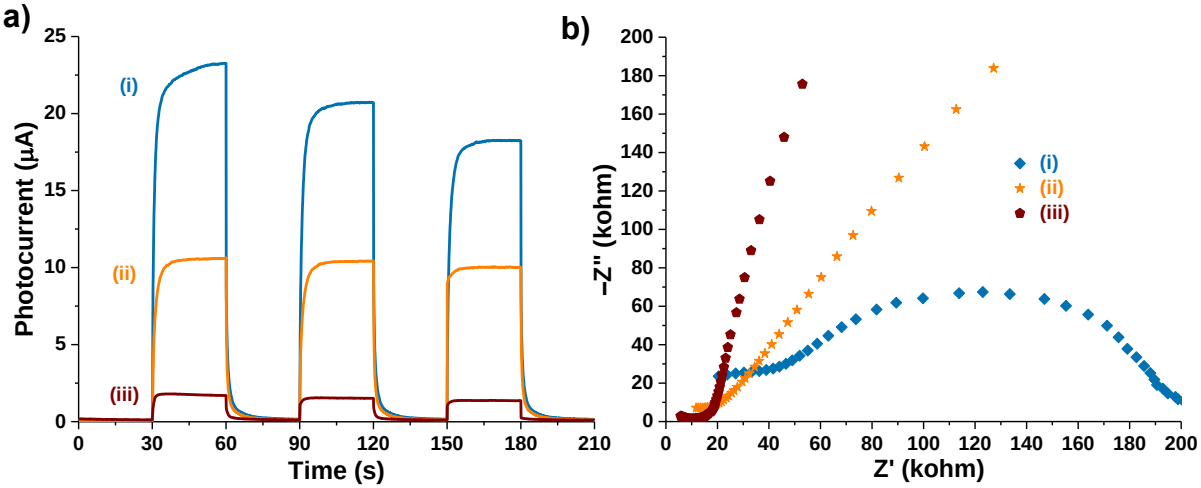

Figure S8: (a) The transient photocurrent responses and (b) EIS Nyquist plots of (i) the hierarchical 70%−Bi_2WO_6/TiO_2-NT nanocomposite, (ii) the Bi_2WO_6/TiO_2 sample prepared without the cellulose template, and (iii) the Bi_2WO_6-TiO_2 sample prepared by physical blend.

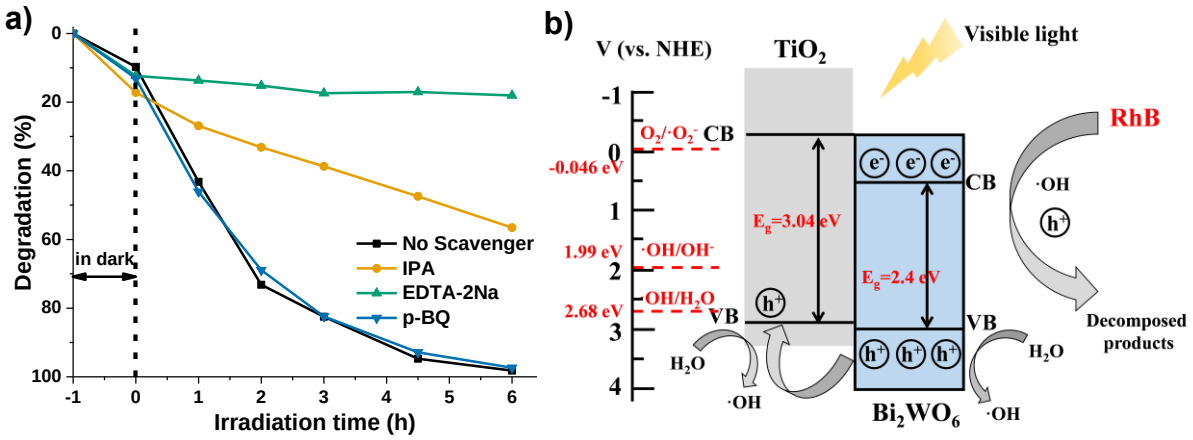

Figure S9: (a) The visible-light (λ > 420 nm) induced photocatalytic degradation profiles towards the RhB pollutant solution (10 mg·L^{-1}) added with IPA, EDTA-2Na, and p-BQ by the hierarchical 70%−Bi_2WO_6/TiO_2-NT nanocomposite. (b) The schematic illustration of the photocatalytic degradation mechanism towards the RhB pollutant by the hierarchical Bi_2WO_6/TiO_2-NT nanocomposite under the irradiation of visible light (λ > 420 nm).

Table S3: Comparison of the hierarchical Bi_2WO_6/TiO_2-nanotube composite with the natural cellulose substance derived Ag_2O-nanoparticle/TiO_2-nanotube composite, g-C_3N_4/TiO_2-nanotube composite, and $H_3PW_{12}O_{40}/TiO_2$ nanocomposite reported by our group.

composites	Light source	morphology	pollutants	K_{app}	Ref.
Bi_2WO_6/ TiO_2-NT	350 W Xe λ > 420 nm	Bi_2WO_6 nanoparticles coated on the TiO_2 nanotubes	RhB Cr(VI)	0.65 h^{-1} 0.52 h^{-1}	This work
Ag_2O-NP/ TiO_2-NT	300 W, Hg	Ag_2O nanoparticles coated on the TiO_2 nanotubes	MB RhB NFCX	0.62 min^{-1} 0.37 min^{-1} 0.29 min^{-1}	[1]
g-C_3N_4/ TiO_2-NT	350 W Xe λ > 420 nm	g-C_3N_4 layer anchored on the TiO_2 nanotube surfaces	MB	0.21 h^{-1}	[2]
$H_3PW_{12}O_{40}$/ TiO_2-NT	300 W, Hg	$H_3PW_{12}O_{40}$ nanoparticles coated on the TiO_2 nanotubes or on the TiO2/cellulose composite sheet	MB	0.54 min^{-1}	[3]

References

1. Lin, Z.; Lu, Y.; Huang, J. *Cellulose* **2019**, *26*, 6683−6700.

2. Lin, Z.; Yu, B.; Huang, J. *Langmuir* **2020**, *36*, 5967−5978.

3. Lin, Z.; Huang, J. *Sep. Purif. Technol.* **2021**, *264*, 118427.